Cell Communication and Signaling

RESEARCH

Open Access

TFE3 fusion proteins promote the progression of *TFE3* rearranged renal cell carcinoma via enhancing chaperone-mediated lipophagy

Wenliang Ma[1†], Yi Chen[2†], Guijuan Chen[3,4†], Lei Yang[3,4], Yanwen Lu[1], Xiang Dong[1], Dongmei Li[3,4] and Weidong Gan[1*]

Abstract

Background *TFE3* rearranged renal cell carcinoma (*TFE3* rRCC), classified as a distinct entity of RCCs, exhibits aggressive biological behavior and possesses unique metabolic characteristics. In the present study, *TFE3* rRCC with high expression of TFE3 fusion proteins was employed to investigate the features of lipid metabolism and its underlying mechanism in cancer progression.

Methods Fluorescence microscope and flow cytometry were employed to detect lipid droplets (LDs). GPO-PAP method and Oil Red O staining were used to quantify triacylglycerol levels. The data for bioinformatics analysis were sourced from GEO and iProX. The biological roles of *TFE3* and *LAMP2A* were investigated by CCK8 assay, EdU staining, seahorse, transwell assay, colony, and sphere formation assay. The regulatory mechanisms involving *TFE3*, *LAMP2A* and *Hsc70* were investigated using western blotting, immunohistochemistry, qRT-PCR, luciferase assays, Co-IP techniques, and ChIP analyses.

Results The level of LDs accumulation in *TFE3* rRCC was relatively low, and the knockdown of *TFE3* led to an increase in LDs accumulation while inhibiting tumor progression. The underlying mechanism revealed that TFE3 fusion proteins inhibited the biosynthesis of LDs within the endoplasmic reticulum by promoting the degradation of DGAT1 and DGAT2 via autophagy. Furthermore, TFE3 fusion proteins upregulated *LAMP2A*, thereby enhancing chaperone-mediated autophagy pathways. The process facilitated the degradation of LDs and promoted oxidative metabolism of long-chain fatty acids in mitochondria.

Conclusions TFE3 fusion proteins facilitated the progression of *TFE3* rRCC through enhancing the degradation of LDs via chaperone-mediated lipophagy. *LAMP2A* could serve as a novel potential prognostic biomarker and therapeutic targets.

Keywords *TFE3* rearranged renal cell carcinoma, Lipid droplets, Autophagy, Lipid metabolism, Cancer progression

[†]Wenliang Ma, Yi Chen and Guijuan Chen contributed equally to this work.

*Correspondence:
Weidong Gan
gwd@nju.edu.cn
[1]Department of Urology, Affiliated Drum Tower Hospital, Medical School of Nanjing University, No. 321 Zhongshan Road, Nanjing, Jiangsu Province 210008, China
[2]Department of Cardiology, Children's Hospital of Nanjing Medical University, Nanjing, Jiangsu 210008, China
[3]State Key Laboratory of Analytical Chemistry for Life Science, Division of Anatomy and Histo-embryology, Medical School, Nanjing University, Nanjing, Jiangsu 210093, China
[4]Jiangsu Key Laboratory of Molecular Medicine, Medical School, Nanjing University, Nanjing, Jiangsu 210093, China

Introduction

TFE3 rearranged renal cell carcinoma (*TFE3* rRCC) is a unique subtype of renal cell carcinoma characterized by high expression of TFE3 fusion proteins. The wild-type *TFE3* is an evolutionarily conserved transcription factor that plays a crucial role in the regulation of various cellular metabolic processes [1–4]. For instance, a high-fat diet has been shown to induce mitochondrial metabolic disorders, systemic abnormalities in glucose and lipid metabolism, as well as increased obesity and diabetes in *TFE3*-knockout mice. Conversely, overexpression of *TFEB* can alleviate the metabolic abnormalities caused by *TFE3*-knockout, indicating a synergistic interaction between *TFE3* and *TFEB*. Skeletal muscle contraction requires substantial energy consumption. Mechanism have demonstrated that intracellular high Ca^{2+} levels promoted nuclear translocation and activation of TFE3, thereby upregulating downstream metabolism-related genes and increasing energy production [5]. These findings suggested that *TFE3* fusion proteins may play a significant role in the metabolic remodeling associated with *TFE3* rRCC. A previous study from our center revealed that the primary energy source of *TFE3* rRCC was mitochondrial oxidative respiration rather than glycolysis. Furthermore, TFE3 fusion proteins enhanced mitochondrial oxidative respiration by transcriptional upregulation of *NMRK2* [6]. While the characteristics of glucose metabolism and mitochondrial oxidative respiration in *TFE3* rRCC have been investigated, lipid metabolism and its underlying mechanisms have not yet been elucidated.

Lipid droplets (LDs) are organelles found in eukaryotic cells that serve as reservoirs for lipids. The dynamic homeostasis of LDs plays a crucial role in various cellular biological processes [7]. Besides energy storage, LDs are vital for mitigating cellular stressors, such as lipotoxicity, endoplasmic reticulum (ER) stress, oxidative stress, and starvation. Furthermore, the biosynthesis and degradation of LDs have been implicated in the pathogenesis of several diseases, including malignant tumors, hepatic steatosis, and neurodegenerative diseases [8]. The biosynthesis of LDs is dependent on diacylglycerol acyltransferases (DGAT), which are anchored within the ER [9–11]. Research has demonstrated that JMJD6 induces the expression of DGAT1, thereby facilitating the accumulation of LDs and promoting cancer progression in clear cell renal cell carcinoma (ccRCC) [12]. Given that the mechanisms underlying tumorigenesis in *TFE3* rRCC differ significantly from those in ccRCC, it is imperative to assess the level of LDs accumulation in *TFE3* rRCC and determine whether the process is regulated by TFE3 fusion proteins.

The level of LDs accumulation is influenced not only by the synthetic processes but also involved by various degradation mechanisms. Current research has identified two degradation pathways, known as lipolysis and lipophagy, respectively [13]. Within the cytoplasm, the core component of LDs, triacylglycerol (TAG), is encased in a phospholipid monolayer and remains resistant to hydrolysis into diacylglycerol and fatty acids (FAs) by adipose triglyceride lipase (ATGL) [14]. Alternatively, LDs may be degraded through the autophagy-lysosome pathways. In this process, LDs were engulfed by autophagosomes and fused with lysosomes, leading to their breakdown facilitated by lysosomal acid lipase (LAL). Additionally, proteins associated with LDs, such as perilipin 2 (PLIN2) and perilipin 3 (PLIN3), can undergo degradation via chaperone-mediated autophagy (CMA), subsequently allowing for hydrolysis by ATGL [15–17]. Wild-type *TFE3* has been shown to promote both autophagy and lysosome biogenesis [3]. Therefore, we aim to clarify the lipid metabolic characteristics and regulatory mechanisms of *TFE3* rRCC to identify new therapeutic targets.

Here, we confirmed the low levels of LDs accumulation in *TFE3* rRCC. The mechanisms suggested that TFE3 fusion proteins facilitated the progression of *TFE3* rRCC through enhancing the degradation of LDs via chaperone-mediated lipophagy. *LAMP2A* could serve as a novel potential prognostic biomarker and therapeutic targets.

Materials and methods

Data collection and bioinformatics analysis

The data for bioinformatics analysis were obtained from the Gene Expression Omnibus (GEO) database and the ProteomeXchange Consortium (iProX). In the datasets of PXD035377 and GSE188885, volcano plots illustrated differentially expressed genes, and both bar charts and dot plots depicted target genes. Bubble plots and bar graphs showed the Gene Ontology (GO) and Gene Set Enrichment Analysis (GSEA) analysis of differentially expressed genes and the Kyoto Encyclopedia of Genes and Genomes (KEGG) enrichment analysis. The statistical analysis and visualization for bioinformatics were performed in R 4.2.1. The visualization operations were carried out using the ggplot2 R package.

Clinical samples collection

Human *TFE3* rRCC paraffin-embedded tissue samples were obtained from thirty patients with complete clinical information confirmed by TFE3 immunohistochemistry (IHC), *FISH*, and transcriptome sequencing at Nanjing Drum Tower Hospital. Matched normal kidney tissues were collected from thirteen patients. The patient cohort consisted of 13 males and 17 females, with a median age of 38 years (range: 22~71 years). According to both tumor size and pathological stage, a total of thirty matched tumor tissue samples were collected from ccRCC patients with a median age of 59 years.

Cell lines and cell culture

HK-2, HEK-293T, and ccRCC cell line 786-O were purchased from the National Infrastructure of Cell Line Resource (Beijing, China) and the Cell Bank of the Chinese Academy of Science (Shanghai, China). The *TFE3* rRCC cell lines UOK120 (*PRCC-TFE3* fusion gene) and UOK109 (*NONO-TFE3* fusion gene) were donated by Professor Maeston Linehan from the National Cancer Institute at the National Institutes of Health. All cell lines were cultured in DMEM (Gibco, USA) supplemented with 10% fetal bovine serum (FBS) (Gibco, USA) and 1% penicillin/streptomycin (Invitrogen, Carlsbad, CA). Cell lines were incubated at 37 °C with 5% CO_2. All cell lines used in this study were authenticated by STR profiling performed by MDHS testing technology (Beijing) prior to experimentation. For all experiments, cells were used between passages 5 and 10 to ensure consistency in cellular behavior and minimize genetic drift. All cell lines were routinely tested for mycoplasma contamination using the Mycoplasma Detection Kit (MCE), and only mycoplasma-free cells were used in the experiments.

Western blot

Total protein was extracted from cells by lysing them with RIPA lysis buffer (Beyotime, P0013C). The lysate was centrifuged, and the supernatant was mixed with loading buffer and heated. Proteins were separated using SDS-PAGE, transferred to a PVDF membrane (Roche, Basel, Switzerland), and blocked with 5% bovine serum albumin (Sigma-Aldrich) for one hour at room temperature. The blots were then incubated with primary antibodies DDDDK-Tag (1:1000, ABclonal, AE092), LC3B (1:500, ABclonal, A7198), DGAT2 (1:1000, ABclonal, A13890), DGAT1 (1:1000, ABclonal, A23077), Hsc70/HSPA8 (1:1000, ABclonal, A0415), LAMP2 (1:1000, ABclonal, A14017), SQSTM1/p62 (1:1000, abcam, ab56416), LAMP2A (1:500, abcam, ab125068), TFE3 (1:1000, abcam, ab93808), β-Actin (ACTB) (1:10000, ABclonal, AC006), GAPDH (1:10000, ABclonal, AC027), and P4HB (PDIA1) (1:1000, ABclonal, A19239) at 4 °C overnight, followed by incubation with secondary antibodies. Protein signals were detected using ECL solution (Millipore) and quantified with ImageJ software (National Institutes of Health). GAPDH, PDIA1 and ACTB were used as an internal control.

RNA isolation and quantitative real-time PCR (qRT-PCR) assay

Total RNA was isolated using the RNA-easy Isolation Reagent (Vazyme, R701-01) following the manufacturer's instructions, and subsequently reverse-transcribed into cDNA using HiScript Q RT SuperMix for qPCR (Vazyme, R122-01). The qRT-PCR was then conducted to quantify cDNA with Taq Pro Universal SYBR qPCR Master Mix (Vazyme, Q712-02). For normalization, 18s rRNA was used as an internal control, and the $2^{-\Delta\Delta Ct}$ method was employed to analyze the relative expression levels of target genes. The primer sequences for the target genes were provided in Additional file 6: Table S1.

IHC staining and scoring

Paraffin-embedded tissues were dewaxed using xylene and rehydrated through a series of gradient ethanol solutions. Endogenous peroxidase activity was inhibited with 3% H_2O_2, followed by antigen retrieval through microwave heating. 10% bovine serum albumin was applied for blocking nonspecific binding. The primary antibody DGAT2 (1:200, ABclonal, A13890), DGAT1 (1:200, ABclonal, A23077), PLIN1 (1:200, ABclonal, A16295), LIPA (LAL) (1:200, ABclonal, A6385), LAMP2 (1:200, ABclonal, A14017), Hsc70/HSPA8 (1:250, ABclonal, A0415), and LAMP2A (1:200, abcam, ab125068) were incubated with the tissue at 4 °C overnight, followed by incubating with the secondary antibody in the dark for two hours. Immunostaining was visualized using diaminobenzidine, and the staining intensity was quantified with ImageJ software.

CCK-8 assay, 5-ethyny-2′-deoxyuridine (EdU) assay, clone formation assay, and transwell assay

Cell proliferation was assessed using the Cell Counting Kit-8 reagent (CCK-8, MCE), with absorbance values measured at 450 nm. EdU (Beyotime, Shanghai, China) was conducted according to the manufacture's protocol. Additionally, 1.5×10^3 cells were seeded into 6-well plates and cultured for two weeks. The number of cell clones formed was determined after staining with crystal violet (Beyotime, C0121), followed by imaging and counting under a microscope. Cell migration and invasion assays were conducted using Transwell chambers (Corning, USA) to evaluate the migratory and invasive capabilities of the cells. The migrated cells were imaged and counted under a 100× microscope.

BODIPY 493/503 staining and quantification of LDs

Prepare 20 mM stock solution by dissolving 5 mg of BODIPY 493/503 powder (Cayman chemical, 25892) in DMSO, stored in the dark at -20 ℃. Dilute the stock solution with PBS at 1:5000 ratio to make 4 μM working solution. Add it to glass-bottom dish seeded with cells, incubated at 37 ℃ for 15 min. Use DAPI (Beyotime, P0131) to stain the nuclei for 10 min. The fluorescence intensity of LDs was analyzed with images from a confocal microscope according these methods based on previous study [18]. Under a 600× oil microscope, 10 random images of cells were captured for each sample. The number of LDs and fluorescence intensity in each cell were then quantified using ImageJ [19]. Finally, the

differences in LDs count and fluorescence intensity among 30 cells per sample were compared. Each sample was subjected to three independent experiments. For the statistical analysis of average fluorescence intensity, 10 random images of cells were captured for each sample under a 600× oil immersion microscope. The fluorescence intensity of each image was then quantified using ImageJ, and the mean value was calculated. The differences in fluorescence intensity among samples were subsequently compared. Each sample was subjected to three independent experiments. Digest cells using trypsin, and cells were collected after centrifugation. Cells were incubated with BODIPY493/503 at 4 μM working solution for 15 min at 37 ℃. The fluorescence intensity of LDs for 1×10^4 cells was analyzed with flow cytometry. For the flow cytometry analysis of LDs, fluorescence peak intensity histograms were obtained from 10,000 cells stained by BODIPY 493/503. The median fluorescence intensity was used as the representative fluorescence intensity for each sample, and the differences among samples were compared.

Apoptosis detection of flow cytometry

Collect cell supernatant and digest cells using trypsin without EDTA. Cells were collected after centrifugation. Resuspend cells with 100 μL binding buffer, 5 μL Annexin V-PE, and 5 μL 7-AAD, and incubate in the dark at room temperature. Add 400 μL binding buffer and perform flow cytometry detection following the manufacturer's instructions (Vazyme, A213-01).

Cell Immunofluorescence

Cells were fixed with 4% paraformaldehyde. The primary antibody was added to a glass-bottom dish, incubated at room temperature for 30 min, and then refrigerated at 4 ℃ overnight. In the next day, the corresponding fluorescent secondary antibodies were added to the glass-bottom dish, incubated at room temperature for two hours. For the statistical analysis of average fluorescence intensity, 10 random images of cells were captured for each sample under a 600× oil immersion microscope. The fluorescence intensity of each image was then quantified using ImageJ, and the mean value was calculated. The differences in fluorescence intensity among samples were subsequently compared. Each sample was subjected to three independent experiments.

Seahorse XFe96 long-chain fatty acid oxidation stress assay

Following the manufacturer's instructions (Agilent, USA), seed cells into the 96-well plate, with 1×10^4 UOK109 cells or 8×10^3 UOK120 cells per well. Then, cells were cultured with the confluency of 80–90% overnight. Incubate the XF calibration solution and hydrate the probe plate overnight. Hydrate the probes in the next day and prepare the detection medium. After washing the cells, place them in a incubator for one hour. Prepare appropriate concentrations of Etomoxir, Oligomycin, FCCP, and Rotenone/Antimycin A (Rot/AA) working solutions and add them to the wells of the probe plate. Set the parameters according to the experimental design, and run the Seahorse. Export the data after the procedure finished. Detect the concentration of protein in each well for normalization with BCA method.

Co-immunoprecipitation (Co-IP) assay

Isolate total proteins from UOK109 and UOK120, and separate the protein into three fractions: 100 μL as Input stored at -20℃, 450 μL as reserve. Add the prepared 450 μL cell lysate to the centrifuge tubes with protein A/G agarose beads incubated with primary antibody or IgG, and incubate overnight at 4 ℃ on a vertical mixer. Centrifuge at 800 rpm and 4 ℃ for 2 min and collect the supernatant. Add 50 μL Loading Buffer to the precipitate, and heat in a metal bath at 100 ℃ for 5 min. Centrifuge at 800 rpm and 4 ℃ for 2 min, and collect the supernatant into new centrifuge tubes for western blotting.

Oil red O staining and quantification of intracellular TAG levels

Once the cells reached the confluency of 80–90%, Oil Red O staining was performed according to the manufacture's instructions (Solarbio, G1262). Measure the absorbance values at 510 nm and compare the differences between groups. Intracellular TAG levels were quantified by following the manufacture's protocol (Jiancheng, A110-1-1).

Dual-luciferase reporter assay

Transfect HEK-293T with the indicated luciferase reporter plasmid pRL-TK and the appropriate plasmid. The dual-luciferase reporter assay kit (Vazyme, DL101-01) was used to measure the luciferase activity of Firefly and Renilla. Calculate the ratio of Firefly to Renilla values.

Tumor sphere formation

Experimental cells were digested with trypsin. Cells were resuspended and counted. Cell suspension with a concentration of 1×10^4 cells/mL was prepared. 100 μL of the above cell suspension was evenly seeded into each well of a low-attachment 96-well plate, with 8 replicates per group. After one to two weeks, tumor spheres were observed under the microscope, and both diameters and volumes were calculated using ImageJ.

Chromatin IP (ChIP)

BersinBio™ ChIP Kit (BersinBio, Bes5001) was used to perform ChIP assay according to the manufacture's protocol. The DNA level was quantified by qRT-PCR, and

the special primers for ChIP are shown in Additional file 6: Table S2.

Plasmid construction, lentivirus, and cell transfection

Both *NONO-TFE3* and *PRCC-TFE3* overexpression plasmid, ligated with pCDH-ECMV-MCS-3×flag-EF1α-T2A-Puro vector plasmid, was constructed by Tsingke Technology (Beijing, China). Promoter sequences for *LAMP2* were obtained from NCBI and subsequently ligated with the pGL3-Basic vector plasmid. The *LAMP2* promoter–luciferase truncation and mutation plasmids were constructed by GENERAL BIOSYSTEM (Chuzhou, China). Sequences for *TFE3*-shRNA and *LAMP2A*-shRNA were acquired from Sigma and ligated with the pLVshRNA-Puro vector plasmid. Cells were transfected with plasmids according to the manufacturer's instruction using jetPRIME (Polyplus-transfection, Shanghai, Illkirch, France). The shRNA sequences and special primers are listed in Additional file 6: Table S3 and S4.

Statistical analysis

The mean ± standard deviation (mean ± S.D.) indicated independent experimental data. Two independent samples compared by the T-test. One-way analysis of variance (ANOVA) was utilized to compare multiple group samples. A *P* value of less than 0.05 was considered statistically significant. Linear regression was employed to analyze the correlation of different molecular expression levels. The coefficient of determination, R^2, was used to indicate correlation. The prognosis of patients was assessed using Kaplan-Meier method. The Log-rank test was used to analyze differences in survival prognosis. Statistical analysis was performed using GraphPad Prism 8.0.1. Adobe Photoshop CC2023 and Adobe Illustrator CC2023 were used for plotting.

Results

TFE3 rRCC exhibited a reduced level of LDs accumulation

By employing BODIPY 493/503 to stain LDs in HK-2, 786-O, UOK109, and UOK120, the results showed that the accumulation of LDs in both UOK109 and UOK120 was significantly lower than that observed in HK-2 (Fig. 1A). Quantitative analysis demonstrated that the levels of LDs accumulation in both UOK109 and UOK120 were markedly reduced compared to those in 786-O (Fig. 1B-C). PLIN1 and PLIN2 are specific proteins associated with LDs modification [17]. Immunofluorescence assays showed that low expression levels of PLIN2 in both UOK109 and UOK120, which aligned with the results obtained from BODIPY 493/503 staining (Fig. 1A and D). Flow cytometry detecting BODIPY 493/503 fluorescence revealed that the fluorescence intensity of LDs in UOK109 and UOK120 was significantly weaker when compared to HK-2 or 786-O (Fig. 1E-F). Additionally, TAG content was notably lower in both UOK109 and UOK120, consistent with their low levels of LDs accumulation (Fig. 1G). IHC analysis demonstrated significantly downregulated levels of PLIN1 and PLIN2 expression in *TFE3* rRCC compared to ccRCC or normal tissue samples (Fig. 1H-I). These results suggested that *TFE3* rRCC exhibited a reduced level of LDs accumulation.

The accumulation of LDs diminished by TFE3 fusion proteins contributed to the enhanced aggressiveness of *TFE3* rRCC

To explore the impact of TFE3 fusion proteins on LDs accumulation in *TFE3* rRCC, BODIPY 493/503 staining demonstrated a significant increase in LDs accumulation in UOK109 and UOK120 following *TFE3* knockdown (Fig. 2A-B). Interestingly, PLIN2 expression was significantly upregulated in UOK109 and UOK120 under similar conditions (Fig. 2A and C). Additionally, fluorescence detection by flow cytometry revealed that the knockdown of *TFE3* significantly enhanced fluorescence intensity of LDs in both cell lines (Fig. 2D-E). The levels of TAG were also significantly elevated in UOK109 and UOK120 after *TFE3* knockdown (Fig. 2F). Furthermore, absorbance values from Oil Red O staining increased for both UOK109 and UOK120 after *TFE3* knockdown, indicating an elevation in TAG accumulation (Fig. 2G). Conversely, LDs accumulation decreased significantly in 786-O after overexpression of the *TFE3* fusion genes (Additional file 3: Figure S3A-E). Collectively, these findings suggested that TFE3 fusion proteins downregulated LDs accumulation in *TFE3* rRCC.

To investigate the effects of TFE3 fusion proteins on the biological behavior of *TFE3* rRCC, both *TFE3* knockdown and overexpression showed significant effects compared to the control group (Additional file 1 and 3: Figures S1A-D and S3A). The CCK-8 assay indicated that silencing *TFE3* significantly suppressed the proliferation of UOK109 and UOK120, whereas overexpression of *TFE3* significantly enhanced the proliferation of 786-O (Additional file 1 and 3: Figures S1E-F and S3F). Tumor sphere formation assay showed that *TFE3*-knockdown significantly inhibited the tumor sphere formation capacity of UOK109 and UOK120; similarly, the colony formation assay indicated that the knockdown of *TFE3* significantly suppressed the colony formation ability of UOK109 and UOK120; conversely, overexpression of *TFE3* yielded opposite results in 786-O (Additional file 1 and 3: Figures S1G-L and S3G-H). Furthermore, the EdU assay demonstrated that overexpression of *TFE3* significantly enhanced DNA replication activity in 786-O (Additional file 3: Figure S3I-J). Flow cytometry-based apoptosis assay indicated that *TFE3*-knockdown significantly increased the apoptosis rate of UOK109 and UOK120 (Additional file 1: Figure S1M-O), and opposite

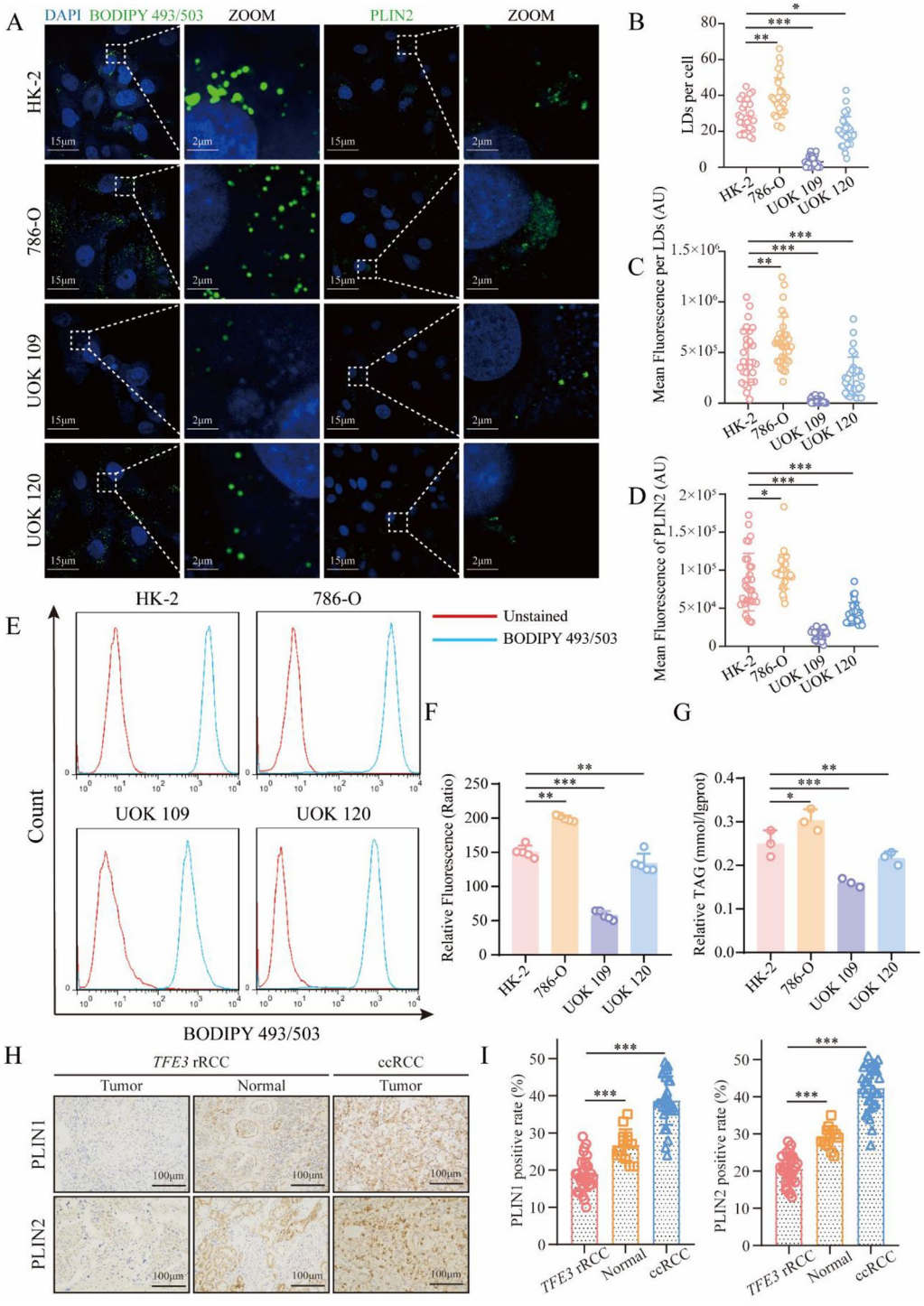

Fig. 1 Low levels of LDs accumulation in *TFE3* rRCC. (**A**) The level of LDs accumulation in HK-2, 786-O, UOK109, and UOK120 were detected using BODIPY 493/503 and PLIN2; (**B**-**C**) The number of LDs and the mean fluorescence intensity were quantitatively analyzed with 30 randomly selected cells in three independent experiments ($n = 30$ cells); (**D**) Quantitative analysis of PLIN2 was performed with 30 randomly selected cells in three independent experiments ($n = 30$ cells); (**E**-**F**) Flow cytometry measured the fluorescence intensity of LDs in HK-2, 786-O, UOK109, and UOK120 ($n = 1 \times 10^4$ cells); (**G**) TAG content in cells was assessed using the GPO-PAP method ($n = 3$); (**H**-**I**) IHC analysis of PLIN1 and PLIN2 protein levels in human *TFE3* rRCC samples ($n = 30$ patients), normal matched samples ($n = 13$ patients), and ccRCC samples ($n = 30$ patients); $^*P < 0.05$; $^{**}P < 0.01$; $^{***}P < 0.001$

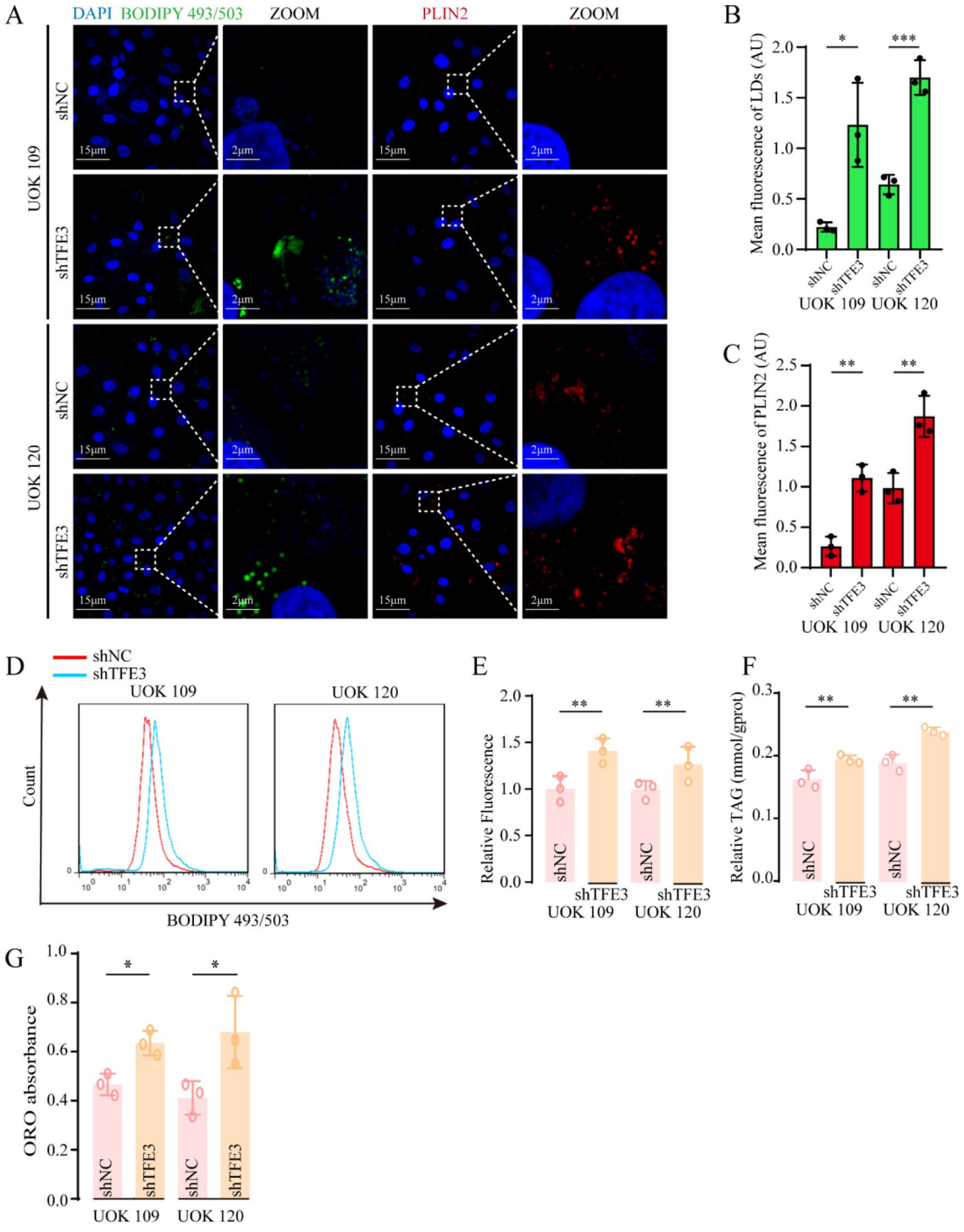

Fig. 2 *TFE3*-knockdown increased LDs accumulation in *TFE3* rRCC. (**A**) The level of LDs accumulation in the control and *TFE3*-knockdown groups of UOK109 and UOK120 were detected using BODIPY 493/503 and PLIN2; (**B**-**C**) The mean fluorescence intensity were quantitatively analyzed ($n = 3$); (**D**-**E**) Flow cytometry analysis of the fluorescence intensity of LDs in the control and *TFE3*-knockdown groups of UOK109 and UOK120 ($n = 3$); (**F**) The GPO-PAP method measured TAG content ($n = 3$); (**G**) Quantitative detection of TAG using Oil Red O staining ($n = 3$); $^{*}P < 0.05$; $^{**}P < 0.01$; $^{***}P < 0.001$

results were observed in 786-O with overexpressed *TFE3* (Additional file 3: Figure S3K-L). Correspondingly, mRNA levels of *BCL2* and *BIRC5* were tested to validate the above results (Additional file 2: Figures S2C-D).

Silencing *TFE3* led to a marked decrease in the migration and invasion capabilities of UOK109 and UOK120 (Additional file 2: Figure S2A-B). The mRNA levels of key regulatory genes, specifically *MMP2* and *MMP9*,

were assessed to validate these findings (Additional file 2: Figure S2C-D). Conversely, overexpression of *TFE3* enhanced the migratory capacity of 786-O cells (Additional file 3: Figure S3M-N). Collectively, these results demonstrated that TFE3 fusion proteins plays a crucial role in influencing the proliferation, survival, and migration and invasion of cancer cells. This suggests that TFE3 fusion proteins were significantly implicated in the aggressiveness of *TFE3* rRCC.

TFE3 fusion proteins regulated the autophagy-lysosome degradation pathway

Under stress conditions like starvation, wild-type TFE3 protein translocated to the nucleus, where it regulated cellular autophagy and lysosome biosynthesis [3]. To investigate whether TFE3 fusion proteins exhibit the same regulatory function, we analyzed transcriptomic dataset GSE188885 from GEO. The analysis revealed that overexpression of *NONO-TFE3* resulted in upregulation of 528 genes and downregulation of 321 genes, while overexpression of *PRCC-TFE3* led to an upregulation of 1511 genes and a downregulation of 1617 genes (Fig. 3A-B). GO analysis showed that the biological processes enriched by upregulated genes resulting from *NONO-TFE3* overexpression included macroautophagy, regulation of autophagy, and lipid catabolism. Furthermore, KEGG pathway analysis indicated that these upregulated genes were associated with pathways related to autophagy and lysosome biogenesis (Fig. 3C). Likewise, GSEA analysis showed that the pathways enriched by upregulated genes from *PRCC-TFE3* overexpression also included those involved in autophagy and lysosome biogenesis (Fig. 3D). To validate the bioinformatics analysis, we observed that mRNA expression levels of *CD63*, *LAMP1*, *VPS18*, *MCOLN1*, *CTSA*, *CTSD*, *CTSF*, *CTSS*, *GAA*, *GBA*, *GLA*, *ATP6V1C1*, *ATP6V0B* and *ATP6V0D2* were significantly reduced following *TFE3*-knockdown in UOK109 and UOK120, as determined by qRT-PCR (Fig. 3E). Conversely, opposite results were observed in 786-O cells overexpressing *TFE3* (Fig. 3F). To further validate the impact of TFE3 fusion proteins on cellular autophagy, we found that *TFE3* knockdown led to a significant upregulation of p62 and a downregulated LC3II/I, indicating an inhibition of autophagic flux in both UOK109 and UOK120 cells following *TFE3*-knockdown (Fig. 3G). We utilize CCK-8 assays to ascertain the optimal concentrations for Bafilomycin A1 (Baf A1) (Figure S4A). After treating tumor cells with Baf A1 for 12 h, we observed a significant increase in intracellular p62 levels, accompanied by a notable decrease in LC3II/I levels, suggesting that *TFE3* knockdown impaired autophagic flux (Fig. 3H). Collectively, these results demonstrated that TFE3 fusion proteins played a crucial role in regulating the autophagy-lysosome degradation pathway in *TFE3* rRCC.

TFE3 fusion proteins suppressed the biosynthesis of LDs in the ER

The ER serves as the site for LDs biosynthesis, where TAG is synthesized by TAG synthases, specifically DGAT1 and DGAT2. The process leads to the gradual accumulation of TAG into a nucleus that eventually buds off into the cytoplasm [11]. The autophagy-induced biosynthesis of LDs relies on DGAT1; notably, inhibition of DGAT1 significantly diminishes LDs accumulation [20]. Previous proteomic data [21] conducted on *TFE3* rRCC revealed that the expression level of DGAT1 in tumor was low, but the difference was not statistically significant (Fig. 4A). Further analysis of *TFE3* rRCC subtypes indicated that the expression level of DGAT1 in *NONO-TFE3* rRCC was significantly lower, while no statistically difference was observed in *PRCC-TFE3* rRCC (Fig. 4B-C). IHC assays displayed that both DGAT1 and DGAT2 exhibited low expression levels in *TFE3* rRCC (Fig. 4D-F). Furthermore, it has been established that ER-localized DGAT2 is essential for LDs biosynthesis as it facilitates TAG accumulation and nucleation [22, 23]. It was crucial to clarify whether TFE3 fusion proteins affected the expression levels of DGAT1 and DGAT2. Consequently, western blot assays showed a significant upregulation of both DGAT1 and DGAT2 after *TFE3*-knockdown; similar findings were obtained using the autophagy inhibitor Baf A1 for 12 h (Fig. 4G-J). These results demonstrated that TFE3 fusion proteins might inhibit LDs synthesis in the ER by promoting the degradation of both DGAT1 and DGAT2 through activating the autophagy-lysosome pathway.

TFE3 fusion proteins facilitated the degradation of cytoplasmic LDs via the autophagy-lysosomal pathway in *TFE3* rRCC

During periods of starvation, cells actively convert TAG stored in LDs into FAs to meet their energy demands. Similarly, starvation triggers autophagy as a mechanism to generate additional energy for cellular functions. Previous study confirmed that intracellular LDs can be degraded through the autophagy-lysosome pathway [24]. To explore whether TFE3 fusion proteins affected lysosome biogenesis and function in *TFE3* rRCC, we observed a significant decrease in the number of lysosomes in UOK109 and UOK120 cells following *TFE3*-knockdown, as determined by 50 nM Lyso-Tracker Red DND-99 (Fig. 5A and C). Furthermore, we used 1 μM Lyso-Sensor™ Green DND-189 to measure lysosomal acidification. The results demonstrated that the levels of lysosomal acidification significantly decreased in UOK109 and UOK120 following

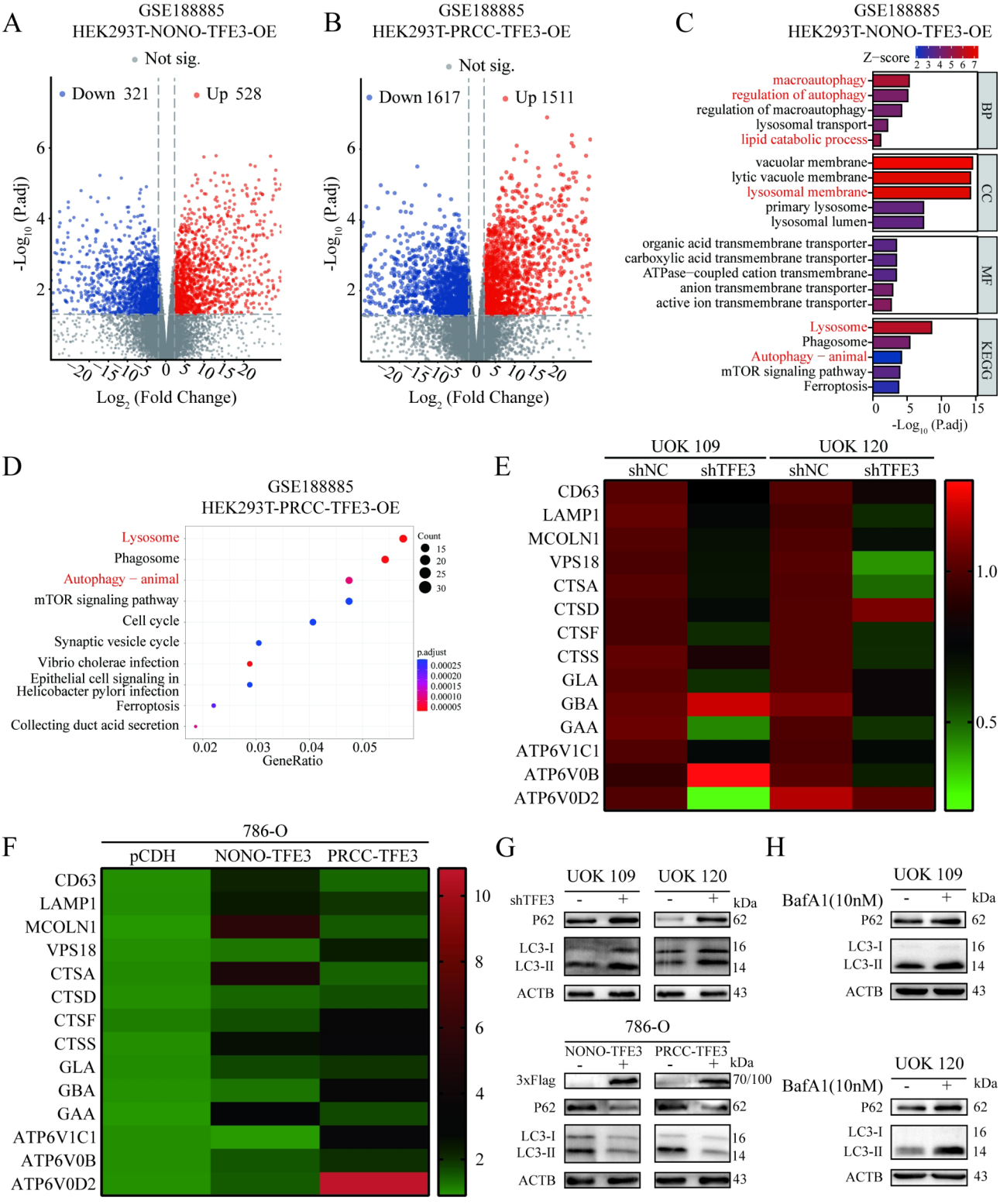

Fig. 3 TFE3 fusion proteins regulated the autophagy-lysosome degradation pathway. (**A**-**B**) The volcano plots displayed the upregulation and down-regulation of genes after the overexpression of *TFE3* fusion genes; (**C**) GO and KEGG analysis revealed pathways enriched in upregulated genes after the overexpression of *NONO-TFE3*; (**D**) GSEA analysis showed pathways enriched in upregulated genes after the overexpression of *PRCC-TFE3*; (**E-F**) The heatmap illustrated mRNA levels of lysosomal marker genes after *TFE3*-knockdown or overexpression. (**G-H**) Western blot determined p62 and LC3II/I in UOK120 and UOK109 after *TFE3*-knockdown or 12-hour treatment with 10 nM Baf A1; **P* < 0.05; ***P* < 0.01; ****P* < 0.001

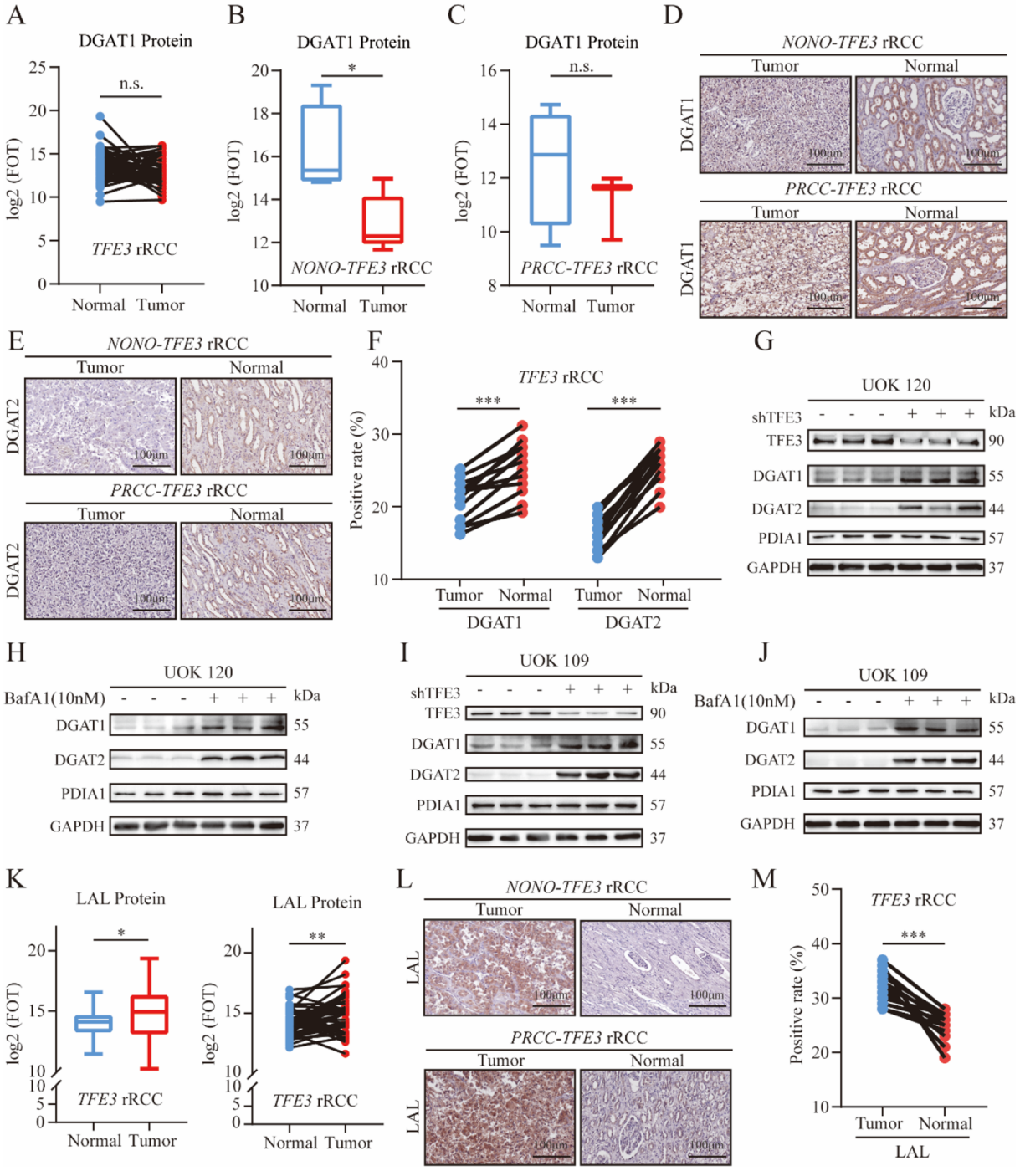

Fig. 4 TFE3 fusion proteins suppressed the biosynthesis of LDs in ER. (**A**) DGAT1 expression levels in matched *TFE3* rRCC samples was analyzed by proteomic data from iProX ($n = 50$ patients); (B-C) DGAT1 expression levels in five *NONO-TFE3* rRCC patients (**B**) and three *PRCC-TFE3* rRCC patients (**C**) were analyzed by proteomic data from iProX; (**D**-**F**) IHC staining and quantified analysis for DGAT1 and DGAT2 in thirteen matched *TFE3* rRCC samples; (**G**-**J**) Western blot was used to determine DGAT1 and DGAT2 in UOK120 and UOK109 after *TFE3*-knockdown or treatment with 10 nM Baf A1 for 12 h ($n = 3$); (**K**) LAL expression level in sixty-seven non-matched *TFE3* rRCC patients or forty-seven matched patients was analyzed by proteomic data from iProX; (**L**-**M**) IHC staining and quantified analysis for LAL in thirteen matched *TFE3* rRCC samples; *$P < 0.05$; **$P < 0.01$; ***$P < 0.001$; n.s.: Not significant

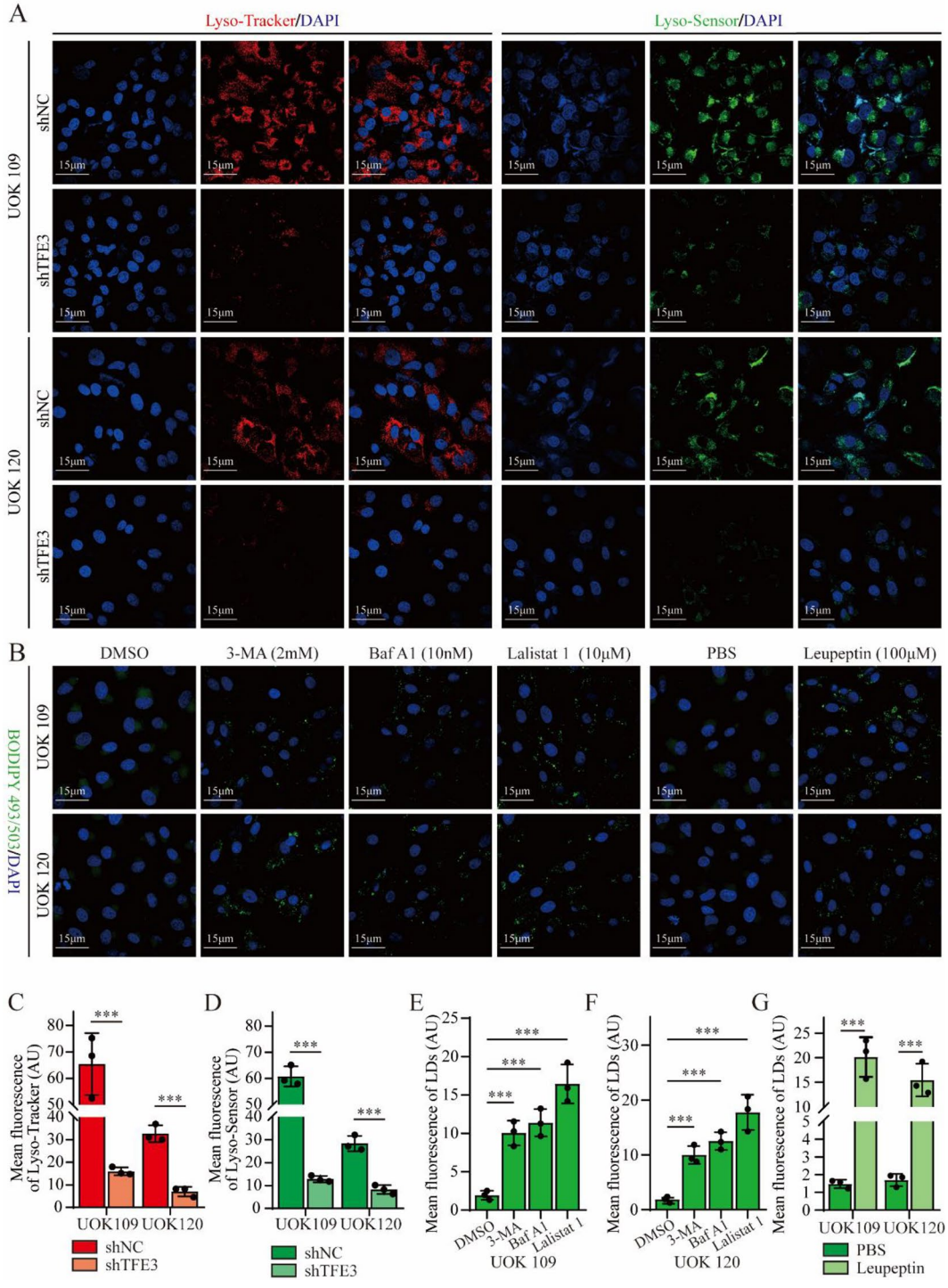

Fig. 5 Suppression of the autophagy-lysosomal degradation pathway increased the level of LDs accumulation. (**A**, **C**-**D**) Lyso-Tracker Red DND-99 detected lysosomes, and Lyso-Sensor™ Green DND-189 measured the acidification of lysosomes ($n = 3$); (**B**, **E**-**G**) The level of LDs accumulation in UOK109 and UOK120 were assessed using BODIPY 493/503 after 12-hour treatments with 3-MA or Baf A1 and 16-hour treatments with Lalistat 1 or Leupeptin ($n = 3$); $^{*}P < 0.05$; $^{**}P < 0.01$; $^{***}P < 0.001$

TFE3 knockdown (Fig. 5A and D). To assess the impact of inhibiting the autophagy-lysosome degradation pathway on accumulation of LDs in *TFE3* rRCC, we utilize CCK-8 assays to ascertain the optimal concentrations for 3-Methyladenine (3-MA) (Figure S4B). Subsequently, tumor cells were treated with 2 mM 3-MA for 12 h, resulting in a significant upregulation in LDs accumulation (Fig. 5B, E-F). The above results revealed that

inhibiting autophagy promoted LDs accumulation in *TFE3* rRCC. Additionally, Baf A1 can impair lysosomal acidification and protein degradation. Treatment with Baf A1 for 12 h resulted in a significant increase in the accumulation of LDs (Fig. 5B, E-F). LAL, encoded by the *LIPA*, is the sole neutral lipid acid hydrolase in lysosomes, and TFEB has been shown to promote lysosome formation and transcriptionally upregulated *LIPA*, thereby enhancing lipid degradation [25, 26]. Transcriptomic analysis revealed that *LIPA* expression levels were significantly elevated in *TFE3* rRCC [27]. Further analysis of previous proteomic data [21] revealed that significantly high expression of LAL in *TFE3* rRCC, which was also corroborated by IHC assays (Fig. 4K-M).We hypothesized that LAL may play a role in LDs degradation in *TFE3* rRCC. To verify this hypothesis, we utilize CCK-8 assays to ascertain the optimal concentrations for LAL inhibitor Lalistat 1 (Figure S4C). Subsequently, tumor cells were treated with 10 μM LAL inhibitor Lalistat 1 for 16 h, resulting in a significant increase in LDs accumulation (Fig. 5B and E-F). Leupeptin is an inhibitor of serine, cysteine, and threonine proteases located within lysosomes. CCK-8 assay was used to ascertain the optimal concentrations for Leupeptin (Figure S4D). To further investigate the involvement of lysosomal proteases in the degradation of LDs, tumor cells were subjected to treatment with 100 μM leupeptin for 16 h, which also resulted in a significant increase in LDs accumulation (Fig. 5B and G). These results suggested that TFE3 fusion proteins facilitated the degradation of cytoplasmic LDs via the autophagy-lysosome pathway in *TFE3* rRCC.

TFE3 fusion proteins facilitated the degradation of LDs by enhancing CMA pathway

CMA is a form of selective autophagy and serve as a degradation pathway for intracellular proteins. Substrate proteins that bind to the chaperone protein Hsc70 in the cytoplasm are transported into the lysosomal lumen by LAMP2A, which CMA activity being associated with LAMP2A [28]. Previous transcriptomic analysis indicated that *LAMP2* mRNA is significantly upregulated in *TFE3* rRCC [27]. We analyzed the GSE188885 dataset and observed a significant increase in *LAMP2* mRNA expression following *TFE3* overexpression (Fig. 6A-B); A similar result was noted in the proteomic data analysis of *TFE3* rRCC (Fig. 6C-D) [21]. Further validation conducted on tumor cells indicated that *TFE3*-knockdown significantly downregulated LAMP2 (Fig. 6G-H), while overexpression of *TFE3* significantly upregulated LAMP2 (Fig. 6K-L). LAMP2 is a crucial lysosomal membrane protein with three isoforms: LAMP2A, LAMP2B, and LAMP2C. Among these isoforms, LAMP2A plays a pivotal role in CMA [29]. We hypothesized that LAMP2A would be significantly upregulated in *TFE3* rRCC. Cell experiment confirmed that the expression levels of LAMP2A were significantly downregulated in UOK109 and UOK120 following *TFE3*-knockdown (Fig. 6E-H), whereas opposite results were observed in 786-O cells with overexpression of *TFE3* (Fig. 6I-L). We extracted whole-cell lysates to confirm the presence of an intact CMA pathway in UOK109 and UOK120 cell lines, and Co-IP experiments demonstrated that there was a direct interaction between Hsc70 and LAMP2A (Fig. 6M). To determine whether TFE3 fusion proteins regulate *LAMP2* transcription, the *LAMP2* promoter sequence was inserted to the pGL3-Basic plasmid. A dual-luciferase reporter gene assay indicated that overexpression of *TFE3* fusion genes significantly enhanced luciferase activity (Fig. 6N). Furthermore, ChIP experiments demonstrated that TFE3 fusion proteins directly bind to the promoter region, thereby upregulating *LAMP2* transcription in tumor cells (Fig. 6O). To clarify the regulatory mechanism, four promoter regions, designated as pGL3-*LAMP2*-P1 (+2000 ~ 486), pGL3-*LAMP2*-P2 (+2000 ~ + 1215), pGL3-*LAMP2*-P3 (+2000 ~ + 1652), pGL3-*LAMP2*-P4 (+2000 ~ + 1869), were cloned into pGL3-Basic plasmid to identify the binding sites of TFE3 fusion proteins. Dual-luciferase reporter assays showed that TFE3 fusion proteins could bind to the region of +1869 ~ +1652 (Fig. 6P). Then, to further determine the actual binding sites, the promoter region of *LAMP2* was cloned into pGL3-Basic plasmids, and mutations were made at 3 putative binding sites, respectively. Dual luciferase assay indicated that the exact sites of TFE3 fusion proteins binding to *LAMP2* was +1706 ~ +1715 (Fig. 6Q). These results indicated that *TFE3* fusion proteins enhanced the CMA pathway by upregulating *LAMP2* transcription.

The hydrophobic core of LDs is surrounded by a phospholipid monolayer, which is modified by specific proteins containing KFERQ-like motifs, such as PLIN2 and PLIN3. These proteins are degraded via the CMA pathway, thereby exposing the neutral hydrophobic lipid core, and facilitating their degradation [15, 16]. To verify that the enhanced CMA pathway promoted LDs degradation, we performed *LAMP2A* knockdown in both UOK109 and UOK120 cells (Fig. 7A-B). Flow cytometry analysis revealed that a significant increase in the fluorescence intensity of LDs following *LAMP2A* knockdown (Fig. 7C-E). Similar results were observed using confocal microscopy with BODIPY 493/503 staining (Fig. 7F-G). To determine whether *LAMP2A* knockdown affects FAs oxidation in tumor cells, we used the standard XF96 long-chain FAs oxidation stress kit to evaluate mitochondrial maximal respiratory capacity dependence on long-chain FAs oxidation in UOK109 and UOK120 cells. The results indicated that *LAMP2A* knockdown significantly reduced the mitochondrial reliance on long-chain FAs oxidation for maximal respiratory capacity (Fig. 7H-I).

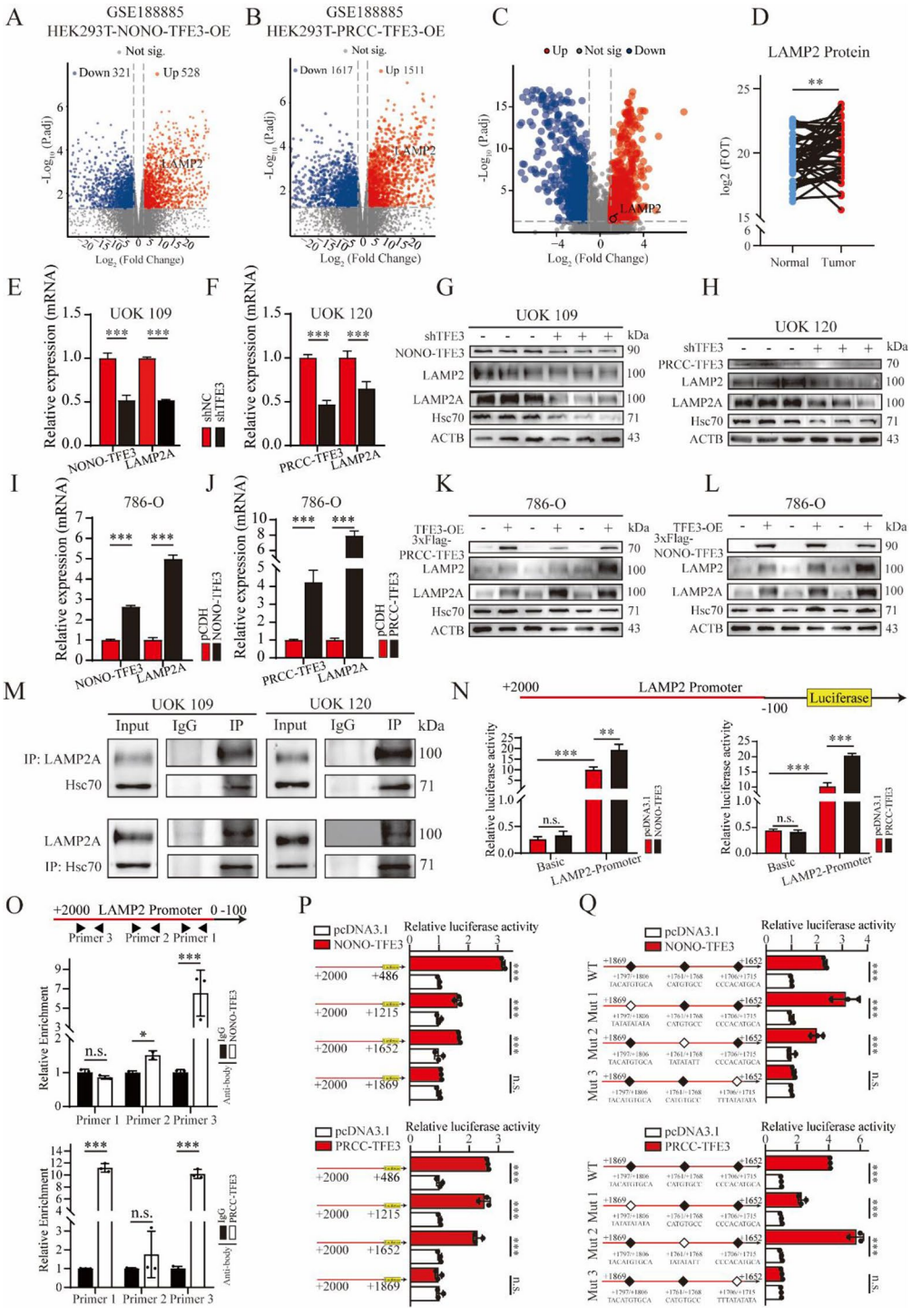

Fig. 6 TFE3 fusion proteins enhanced CMA pathways. (**A**-**B**) The volcano plots demonstrated that the overexpression of *TFE3* fusion genes upregulated *LAMP2*; (**C**-**D**) High levels of LAMP2 expression in matched *TFE3* rRCC samples via proteomic data from iProX ($n = 50$ patients); (**E**-**H**) Western blot and qRT-PCR detection of LAMP2, LAMP2A, and Hsc70 after *TFE3*-knockdown in UOK109 and UOK120 cells ($n = 3$); (**I**-**L**) Western blot and qRT-PCR detection of LAMP2, LAMP2A, and Hsc70 after *TFE3*-overexpression in 786-O ($n = 3$); (**M**) Co-IP validated the interaction between LAMP2A and Hsc70 in UOK109 and UOK120 cells; (**N**) HEK-293T cells were transfected with *LAMP2* full-length promoter and *TFE3* fusion genes plasmids, and the luciferase activity was determined using a dual luciferase reporter assay after 48 h ($n = 3$); (**O**) ChIP assay and qRT-PCR were used to determine the binding affinity of TFE3 fusion proteins to *LAMP2* promoter regions ($n = 3$); (**P**) The luciferase activity was determined after transfecting with *LAMP2* promoter–luciferase truncations plasmids ($n = 3$); (**Q**) The wild-type or mutant TFE3 fusion proteins potential binding sites of *LAMP2* promoter plasmids were designed for Dual luciferase assay ($n = 3$); $^{*}P < 0.05$; $^{**}P < 0.01$; $^{***}P < 0.001$

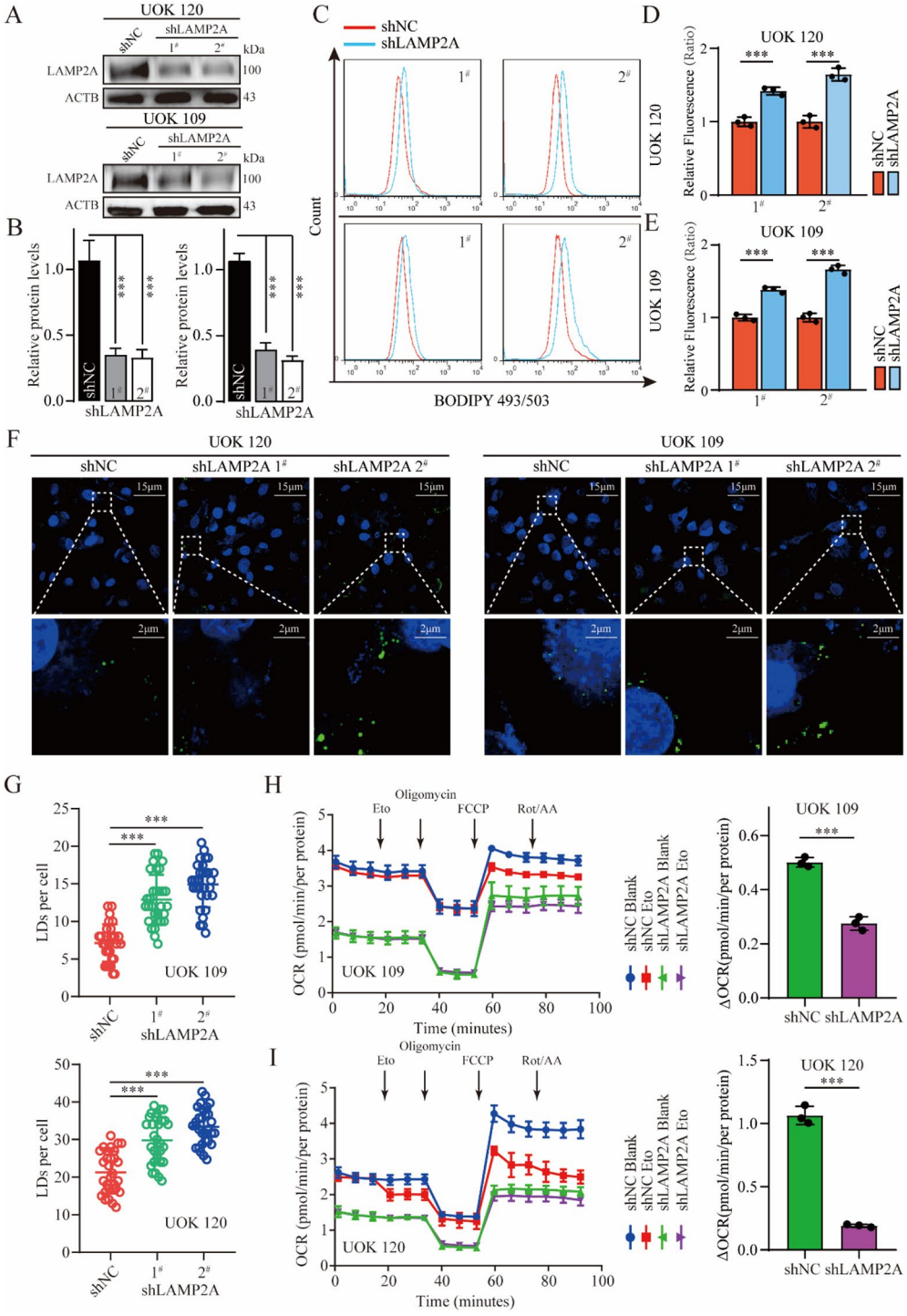

Fig. 7 *LAMP2A*-knockdown suppressed the degradation of LDs. (**A**-**B**) The protein levels of LAMP2A expression were detected after transfection with shLAMP2A ($n = 3$); (**C**-**E**) Flow cytometry analyzed the fluorescence intensity of LDs stained with BODIPY 493/503 ($n = 1 \times 10^4$ cells); (**F**-**G**) The level of LDs accumulation was detected using BODIPY 493/503 in three independent experiments ($n = 30$ cells); (**H**-**I**) The standard XF96 long-chain FAs oxidation stress kit was employed to assess the dependence of mitochondrial maximal respiratory capacity on long-chain FAs oxidation in UOK109 and UOK120 ($n = 5$); Eto: Etomoxir; Rot/AA: Rotenone/antimycin A; *$P < 0.05$; **$P < 0.01$; ***$P < 0.001$

These results suggested that TFE3 fusion proteins transcriptionally upregulated *LAMP2A* and enhanced CMA activity to facilitate LDs degradation, thus promoting mitochondrial long-chain FAs oxidation to supply abundant energy for tumor progression in *TFE3* rRCC.

Enhanced expression of *LAMP2A* facilitated LDs degradation and the progression of *TFE3* rRCC

To investigate the impact of *LAMP2A* on the biological behavior of *TFE3* rRCC, IHC analysis showed significantly elevated levels of LAMP2A expression in *TFE3* rRCC compared to ccRCC (Fig. 8A-C). Furthermore, both LAMP2 and Hsc70 were found to be highly expressed (Fig. 8A-C), corroborating our findings from cell experiment. Correlation analysis revealed a strong association between the TFE3 fusion proteins and LAMP2A or Hsc70 in tumor tissues (Fig. 8D-E). Kaplan-Meier analysis, using the median expression levels of LAMP2A in tumor tissues as a cutoff value, revealed that patients exhibiting high levels of LAMP2A had significantly pooper overall survival (OS) and progression-free survival (PFS) compared to those with low expression levels (Fig. 8F-G). The CCK-8 assay indicated that the knockdown of LAMP2A significantly inhibited the proliferation of UOK109 and UOK120 cells (Additional file 5: Figure S5A-C). Consistent with these findings, sliencing *LAMP2A* significantly decreased the migration and invasion capabilities of tumor cells (Additional file 5: Figure S5D-H). A series of rescue experiments were performed to confirm the hypothesis of TFE3 fusion proteins mediating *TFE3* rRCC progression and LDs degradation through LAMP2A (Additional file 5: Figure S5I-N). These results suggested that high expression of LAMP2A enhanced both LDs degradation and the progression of *TFE3* rRCC.

Discussion

LDs in the cytoplasm were first identified in the late 19th century, however, research on LDs progressed slowly throughout the following century, leaving their formation processes and functions largely unexplored [8]. Over the past three decades, researches have demonstrated that intracellular LDs are organelles critical for alleviating cellular stress, including lipotoxic, ER stress, oxidative stress, and starvation. Furthermore, the dysregulation of the dynamic balance of intracellular LDs has been implicated in the progression of multiple diseases [7, 9]. In this study, we demonstrated that the accumulation of LDs was relatively low in *TFE3* rRCC. Knocking down *TFE3* resulted in increased LDs accumulation and inhibited tumor cell proliferation, migration, and invasion in *TFE3* rRCC. The molecular mechanisms revealed that TFE3 fusion proteins suppressed the expression of DGAT1 and DGAT2, which were essential for LDs biosynthesis in ER. Additionally, TFE3 fusion proteins promoted autophagy and lysosomal synthesis, thereby enhancing the degradation of intracellular LDs. Inhibiting lysosome activity or knocking down *LAMP2A*, which suppressed CMA, led to increased accumulation of intracellular LDs as well as inhibition of tumor cell proliferation, migration, and invasion. Therefore, our study highlighted the role of dysregulated LD metabolism and CMA pathways in *TFE3* rRCC, suggesting that *LAMP2A* could serve as potential therapeutic targets.

However, numerous studies have confirmed a high level of LDs accumulation in various malignant tumor [30]. Tumor cells require LDs to supply essential raw materials for membrane synthesis during proliferation. Previous research has identified two primary mechanisms through which LDs in tumor cells facilitated tumor progression. Firstly, LDs accumulation in tumor cells can mitigate various stress conditions during tumor proliferation, such as hypoxia and starvation; secondly, the metabolic activities of tumor cells necessitate substantial amounts of energy and raw materials provided by LDs, such as, FAs [31, 32]. Research has confirmed that HIF-2α promotes the expression of PLIN2 and leads to elevated levels of LDs accumulation in ccRCC. High expression levels of PLIN2 are essential for maintaining tumor cell survival and ER stress homeostasis; furthermore, increased LDs accumulation in tumor cells enhances tumor cell proliferation and stress resistance [33]. Zhou et al. identifies JMJD6 as a key pathogenic gene associated with ccRCC using unbiased siRNA screening technology and considered DGAT1 as a significant downstream effector gene of JMJD6 through ChIP-seq and transcriptomics, and silencing JMJD6 or DGAT1, respectively, inhibited tumor growth and LDs accumulation, proposing a new therapeutic method for ccRCC [12]. Our study demonstrated low expression levels of DGAT1 and DGAT2 in *TFE3* rRCC. Additionally, cellular experiments confirmed that *TFE3* knockdown or autophagy inhibition led to an upregulation of DGAT1 and DGAT2 expression. These findings suggested that TFE3 fusion proteins may promote the degradation of DGAT1 and DGAT2 by enhancing the autophagic degradation pathway. This may be one of the reasons for the low level of LDs accumulation phenotype observed in *TFE3* rRCC. Glioblastoma shared a similar lipid phenotype with ccRCC, characterized by high level of LDs accumulation in tumor tissues. Study has confirmed that high expression of DGAT1 promoted the synthesis of LDs in the ER, and *DGAT1*-knockdown significantly reduced LDs accumulation and induced tumor cell apoptosis [34]. The mechanism revealed *DGAT1*-knockdown promoted LDs breakdown to produce acylcarnitine, and it entered the mitochondria for oxidative degradation and increased mitochondrial ROS levels, which caused mitochondrial damage and cell

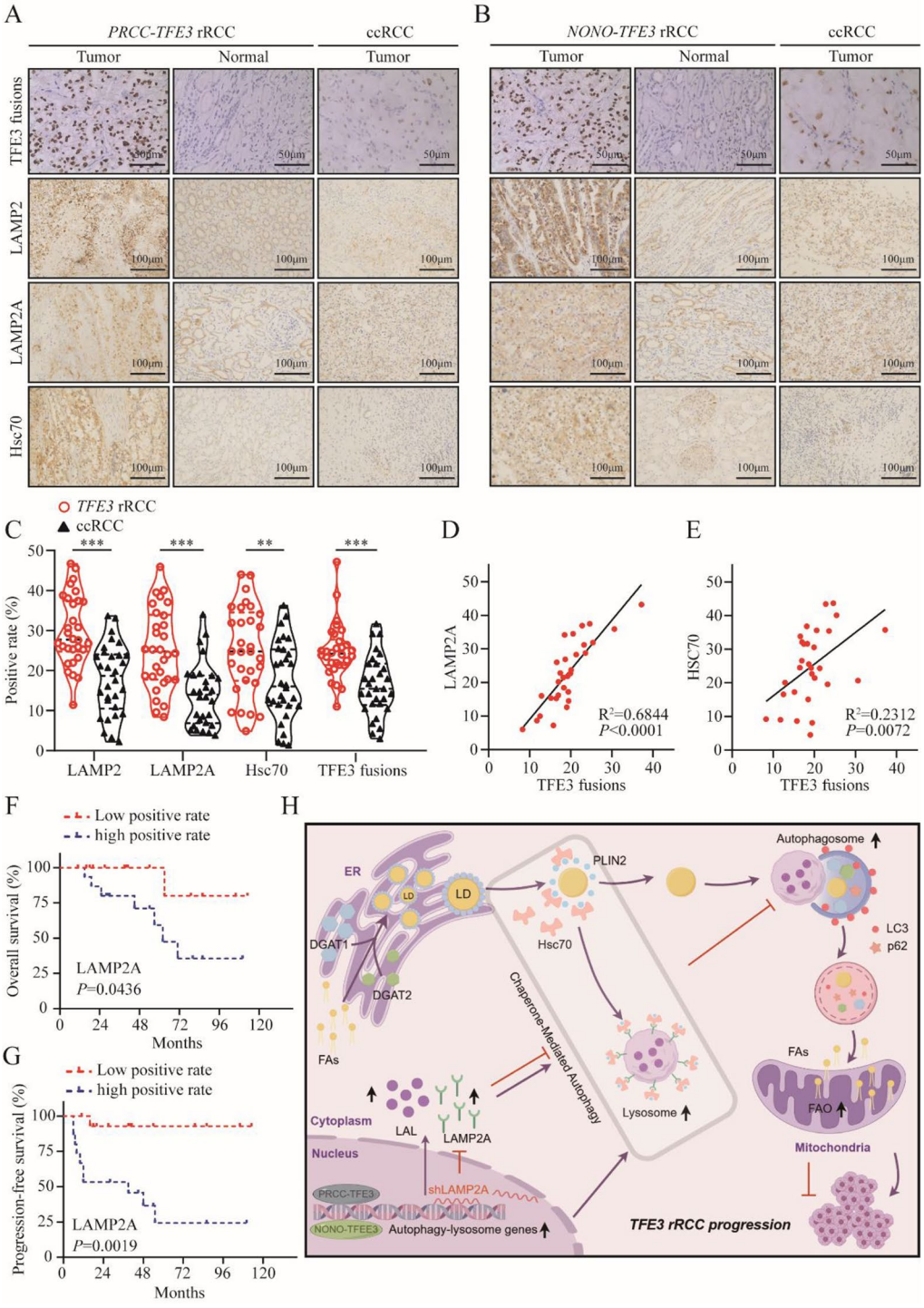

Fig. 8 Patients with high LAMP2A expression had poor prognosis. (**A**-**C**) IHC analysis of LAMP2, LAMP2A, Hsc70, and TFE3 fusion proteins levels in human *TFE3* rRCC ($n = 30$ patients) and ccRCC ($n = 30$ patients) tumor samples; (**D**-**E**) Correlation analysis between the expression levels of TFE3 fusion proteins and LAMP2A or Hsc70 in *TFE3* rRCC ($n = 30$ patients); (**F**-**G**) Kaplan-Meier analysis of overall survival and progression-free survival between *TFE3* rRCC patients with low and high LAMP2A protein expression levels ($n = 30$ patients); (**H**) Schematic diagram for the mechanisms of TFE3 fusion proteins enhancing autophagy-mediated lipid droplets degradation to promote the growth of *TFE3* rRCC; *$P < 0.05$; **$P < 0.01$; ***$P < 0.001$

apoptosis [34]. Thus, LDs accumulation in the cytoplasm can alleviate mitochondrial oxidative stress, maintain cell survival, and promote tumor cell proliferation and metastasis.

Intracellular LDs not only promoted tumor proliferation by alleviating various cellular stress but also provided energy for tumor cells invasion and metastasis [35, 36]. Currently, scholars believed that the tumor microenvironment was acidic and hypoxic, which caused high level of CD36 expression and enhanced the uptake of long-chain free FAs to synthesize LDs [35]. Mechanism has found that acidic tumor microenvironment induced tumor cells to secrete TGF-β2, which upregulated CD36 and increased nuclear translocation of Smad2, and Smad2 upregulated target genes associated with epithelial-to-mesenchymal transition to resist anoikis, thereby promoting tumor invasion and metastasis [35]. In addition, the KRAS/HSL axis regulated the degradation of cytoplasmic LDs in normal pancreatic ductal cells, however, KRAS mutation significantly increased LDs accumulation and decreased FAs oxidation in pancreatic ductal adenocarcinoma [36]. As the invasion and metastasis ability of tumor cells increased, both LDs degradation and FAs oxidation capacities were significantly enhanced to adapt to the high-energy consumption state [36]. Cytoplasmic LDs are subsequently degraded by HSL to increase ATP production during tumor cell invasion and metastasis, thereby driving the energy-intensive process of tumor cell invasion and metastasis. In summary, research data indicated that DGAT1, PLIN2, and HSL may be potential targets for anti-tumor therapy. However, further research is needed to validate these therapeutic targets and strategies.

Multiple pathways were involved in the degradation of cytoplasmic LDs, and abnormalities in these degradation mechanisms can affect LDs accumulation levels. The pathways for LDs degradation can be classified into two types: the neutral lipolysis pathway involved the sequential hydrolysis of triacylglycerol, diacylglycerol, and monoacylglycerol into FAs and glycerol, mediated by triacylglycerol lipase, hormone-sensitive lipase, and monoacylglycerol lipase; the alternative pathway was acidic lipolysis, in which LDs were hydrolyzed by LAL within lysosomes [13]. LAL showed peak activity at a lysosomal pH of 4.5 to 5.0, and it can hydrolyze various lipid substrates, including triacylglycerol, diacylglycerol, cholesteryl esters and retinyl esters [37–39]. *TFEB* can transcriptionally upregulated LIPA [40]. Due to the overlap in the transcriptional activities of *TFE3* and *TFEB*, the transcriptional regulation of *LIPA* by *TFE3* merits further experimental confirmation [41]. Our study demonstrated that the levels of LAL protein and mRNA expression in *TFE3* rRCC were significantly higher than those in adjacent non-cancerous tissues. Inhibiting LAL enzyme activity in lysosomes led to a substantial increase in LDs accumulation, suggesting that TFE3 fusion proteins may enhance the degradation of LDs by regulating LAL activity. Furthermore, the human *TFE3* homolog gene *HLH-30* has been demonstrated to transcriptionally activate lysosomal lipolysis and autophagy pathways in *Caenorhabditis elegans* [42], providing additional evidence that the *TFE3* can regulate the acidic lipolysis pathway.

In 2009, Singh et al. discovered that cytoplasmic LDs can be degraded via the autophagy pathway, termed "lipophagy" [24]. The molecules involved in recruiting proteins for the degradation of LDs in the cytoplasm, as well as the carrier proteins that bind to LDs, have not yet been fully elucidated. Nevertheless, the essential step of LDs degradation in lipophagy was autophagosomes fused with lysosomes to form autolysosomes, but the fusion mechanism was still not well understood [13]. Our study confirmed that the autophagy pathway was activated following *TFE3* overexpression. In contrast, *TFE3* knockdown resulted in the inhibition of the autophagy pathway and a significant increase in LDs accumulation. This suggested that the autophagy pathway was involved in the degradation of LDs. Further investigation revealed that the knockdown of *TFE3* significantly inhibited both the biosynthesis and function of lysosomes in tumor cells. Consequently, TFE3 fusion proteins obstructed the autophagy pathway by impairing lysosome formation, which prevented the degradation of LDs in the cytoplasm. Autophagy also included CMA, which was involved in the degradation of neutral lipids by degrading LDs-related proteins [15]. PLIN2 and PLIN3 were protein markers of cytoplasmic LDs, providing protection against degradation by cytoplasmic lipases and autophagosomes. However, they were target proteins of CMA. Our study confirmed that TFE3 fusion proteins can enhance CMA to degrade LDs-associated proteins, thus promoting the degradation of LDs. Given the elevated expression of LAMP2A in *TFE3* rRCC, LAMP2A inhibitors could be explored as therapeutic agents. Although direct inhibitors of LAMP2A are currently limited, CMA pathway modulators, such as atypical retinoid 7, could be tested for their efficacy in inhibiting tumor aggressiveness [43]. Additionally, stabilizing LAMP2A might enhance CMA, and interfering the stability of LAMP2A could also serve as potential therapeutic targets. *TFE3* rRCC displayed unique lipid metabolic characteristics. Investigating the underlying molecular mechanisms may enhance our understanding of the pathogenesis of *TFE3* rRCC and facilitate the identification of new diagnostic biomarkers and therapeutic targets. Regrettably, the absence of animal experiments limits the translational potential of our findings, as in vivo physiological and pathological responses cannot be fully replicated in vitro. We will

continue our efforts to isolate and extract primary cells and conduct animal experiments to further validate and expand our current research findings.

Conclusion

Our study revealed that the level of LDs accumulation in *TFE3* rRCC is relatively low. Notably, the knockdown of *TFE3* resulted in an increased LDs accumulation while inhibiting tumor progression. The underlying mechanism demonstrated that TFE3 fusion proteins suppressed the biosynthesis of LDs in the ER by enhancing DGAT1 and DGAT2 degradation via autophagy. Furthermore, TFE3 fusion proteins bound to the promoter region of *LAMP2* and upregulated *LAMP2A* to enhance CMA pathways, thereby promoting LDs degradation in the cytoplasm and the long-chain FAs oxidative in mitochondria (Fig. 8H). High expression levels of LAMP2A facilitated the proliferation of *TFE3* rRCC. Our findings help better understand the biological function of TFE3 fusion proteins in lipid metabolism of *TFE3* rRCC and provide a rationale for diagnosis and treatment in *TFE3* rRCC.

Abbreviations

RCC	Renal cell carcinoma
ccRCC	Clear cell renal cell carcinoma
LDs	Lipid droplets
TFE3 rRCC	TFE3 rearranged renal cell carcinoma
ER	Endoplasmic reticulum
DGAT	Diacylglycerol acyltransferases
TAG	Triacylglycerol
FAs	Fatty acids
ATGL	Adipose triglyceride lipase
LAL	Lysosomal acid lipase
CMA	Chaperone-mediated autophagy
PLIN1	Perilipin 1
iProX	ProteomeXchange Consortium
Co-IP	Co-immunoprecipitation
ChIP	Chromatin IP
GEO	Gene Expression Omnibus
KEGG	The Kyoto Encyclopedia of Genes and Genomes

Supplementary Information

The online version contains supplementary material available at https://doi.org/10.1186/s12964-025-02117-y .

Supplementary Material 1

Supplementary Material 2

Supplementary Material 3

Acknowledgements

We are grateful to Dr. W. Marston Linehan from the National Cancer Institute in America for giving us the UOK109 and UOK120 cell lines. We really thank The Translational Medicine Core Facilities, Medical School, Nanjing University, Nanjing, China, for providing the experimental equipment. We truly thank the TCGA and GEO working groups for generously sharing their data.

Author contributions

YC, GJC, DML, WDG, and WLM designed the study and conceived the project. YC, GJC, and WLM collected the data from several databases. YC, GJC, and WLM drafted the manuscript. LY, XD, and YWL reviewed the results and revised the manuscript. All authors read and approved the final manuscript.

Funding

This research was supported by the Project of Natural Science Foundation of Jiangsu Province of China (BK20221444), the Medical Research Project of Jiangsu Province Health Commission (No. ZD2022013), and the Beijing Ronghe Medical Development Foundation.

Data availability

No datasets were generated or analysed during the current study.

Declarations

Ethics approval and consent to participate

All patients have written an informed consent form, and the study protocol has acquired official approval from the Institutional Review Board of Affiliated Drum Tower Hospital, Medical School of Nanjing University.

Consent for publication

Not applicable.

Competing interests

The authors declare no competing interests.

Received: 13 November 2024 / Accepted: 21 February 2025
Published online: 06 March 2025

References

1. Judge A, Dodd MS. Metabolism Essays Biochem. 2020;64(4):607–47.
2. Li X, Chen Y, Gong S, et al. Emerging roles of TFE3 in metabolic regulation. Cell Death Discov. 2023;9(1):93.
3. Martina JA, Diab HI, Lishu L, et al. The nutrient-responsive transcription factor TFE3 promotes autophagy, lysosomal biogenesis, and clearance of cellular debris. Sci Signal. 2014;7(309):ra9.
4. Pastore N, Vainshtein A, Klisch TJ, et al. TFE3 regulates whole-body energy metabolism in Cooperation with TFEB. EMBO Mol Med. 2017;9(5):605–21.
5. Martina JA, Diab HI, Brady OA, et al. TFEB and TFE3 are novel components of the integrated stress response. Embo J. 2016;35(5):479–95.
6. Chen Y, Yang L, Lu Y et al. Up-regulation of NMRK2 mediated by TFE3 fusions is the key for energy metabolism adaption of Xp11.2 translocation renal cell carcinoma. Cancer Lett. 2022:215689.
7. Henne WM, Reese ML, Goodman JM. The assembly of lipid droplets and their roles in challenged cells. Embo J. 2018;37(12).
8. Zadoorian A, Du X, Yang H. Lipid droplet biogenesis and functions in health and disease. Nat Rev Endocrinol. 2023;19(8):443–59.
9. Gao M, Huang X, Song BL, et al. The biogenesis of lipid droplets: lipids take center stage. Prog Lipid Res. 2019;75:100989.
10. Olzmann JA, Carvalho P. Dynamics and functions of lipid droplets. Nat Rev Mol Cell Biol. 2019;20(3):137–55.
11. Walther TC, Chung J, Farese RV. Jr. Lipid droplet biogenesis. Annu Rev Cell Dev Biol. 2017;33:491–510.
12. Zhou J, Simon JM, Liao C, et al. An oncogenic JMJD6-DGAT1 axis tunes the epigenetic regulation of lipid droplet formation in clear cell renal cell carcinoma. Mol Cell. 2022;82(16):3030–e448.
13. Zechner R, Madeo F, Kratky D. Cytosolic lipolysis and lipophagy: two sides of the same coin. Nat Rev Mol Cell Biol. 2017;18(11):671–84.
14. Haemmerle G, Lass A, Zimmermann R, et al. Defective lipolysis and altered energy metabolism in mice lacking adipose triglyceride lipase. Science. 2006;312(5774):734–7.
15. Kaushik S, Cuervo AM. Degradation of lipid droplet-associated proteins by chaperone-mediated autophagy facilitates lipolysis. Nat Cell Biol. 2015;17(6):759–70.
16. Loix M, Wouters E, Vanherle S, et al. Perilipin-2 limits remyelination by preventing lipid droplet degradation. Cell Mol Life Sci. 2022;79(10):515.
17. Straub BK, Gyoengyoesi B, Koenig M, et al. Adipophilin/perilipin-2 as a lipid droplet-specific marker for metabolically active cells and diseases associated with metabolic dysregulation. Histopathology. 2013;62(4):617–31.
18. Papsdorf K, Miklas JW, Hosseini A, et al. Lipid droplets and peroxisomes are co-regulated to drive lifespan extension in response to mono-unsaturated fatty acids. Nat Cell Biol. 2023;25(5):672–84.

19. Liu Y, Wang T, Ji YJ, et al. A C9orf72-CARM1 axis regulates lipid metabolism under glucose starvation-induced nutrient stress. Genes Dev. 2018;32(21–22):1380–97.
20. Wilcock DJ, Badrock AP, Wong CW, et al. Oxidative stress from DGAT1 oncoprotein Inhibition in melanoma suppresses tumor growth when ROS defenses are also breached. Cell Rep. 2022;39(12):110995.
21. Qu Y, Wu X, Anwaier A, et al. Proteogenomic characterization of MiT family translocation renal cell carcinoma. Nat Commun. 2022;13(1):7494.
22. Chun J, Riella CV, Chung H, et al. DGAT2 Inhibition potentiates lipid droplet formation to reduce cytotoxicity in APOL1 kidney risk variants. J Am Soc Nephrol. 2022;33(5):889–907.
23. Xu N, Zhang SO, Cole RA, et al. The FATP1-DGAT2 complex facilitates lipid droplet expansion at the ER-lipid droplet interface. J Cell Biol. 2012;198(5):895–911.
24. Singh R, Kaushik S, Wang Y, et al. Autophagy regulates lipid metabolism. Nature. 2009;458(7242):1131–5.
25. Emanuel R, Sergin I, Bhattacharya S, et al. Induction of lysosomal biogenesis in atherosclerotic macrophages can rescue lipid-induced lysosomal dysfunction and downstream sequelae. Arterioscler Thromb Vasc Biol. 2014;34(9):1942–52.
26. Li F, Zhang H. Lysosomal acid lipase in lipid metabolism and beyond. Arterioscler Thromb Vasc Biol. 2019;39(5):850–56.
27. Sun G, Chen J, Liang J, et al. Integrated exome and RNA sequencing of TFE3-translocation renal cell carcinoma. Nat Commun. 2021;12(1):5262.
28. Dice JF. Chaperone-mediated autophagy. Autophagy. 2007;3(4):295–9.
29. Qiao L, Hu J, Qiu X, et al. LAMP2A, LAMP2B and LAMP2C: similar structures, divergent roles. Autophagy. 2023;19(11):2837–52.
30. Cruz ALS, Barreto EA, Fazolini NPB, et al. Lipid droplets: platforms with multiple functions in cancer hallmarks. Cell Death Dis. 2020;11(2):105.
31. Cui Y, Man S, Tao J et al. The lipid droplet in cancer: from being a tumor-supporting hallmark to clinical therapy. Acta Physiol (Oxf). 2024:e14087.
32. Luo W, Wang H, Ren L, et al. Adding fuel to the fire: the lipid droplet and its associated proteins in cancer progression. Int J Biol Sci. 2022;18(16):6020–34.
33. Qiu B, Ackerman D, Sanchez DJ, et al. HIF2α-Dependent lipid storage promotes Endoplasmic reticulum homeostasis in Clear-Cell renal cell carcinoma. Cancer Discov. 2015;5(6):652–67.
34. Cheng X, Geng F, Pan M, et al. Targeting DGAT1 ameliorates glioblastoma by increasing fat catabolism and oxidative stress. Cell Metab. 2020;32(2):229–e428.
35. Corbet C, Bastien E, Santiago de Jesus JP, et al. TGFβ2-induced formation of lipid droplets supports acidosis-driven EMT and the metastatic spreading of cancer cells. Nat Commun. 2020;11(1):454.
36. Rozeveld CN, Johnson KM, Zhang L, et al. KRAS controls pancreatic Cancer cell lipid metabolism and invasive potential through the lipase HSL. Cancer Res. 2020;80(22):4932–45.
37. Grumet L, Eichmann TO, Taschler U, et al. Lysosomal acid lipase hydrolyzes retinyl ester and affects retinoid turnover. J Biol Chem. 2016;291(34):17977–87.
38. Sheriff S, Du H, Grabowski GA. Characterization of lysosomal acid lipase by site-directed mutagenesis and heterologous expression. J Biol Chem. 1995;270(46):27766–72.
39. Warner TG, Dambach LM, Shin JH, et al. Purification of the lysosomal acid lipase from human liver and its role in lysosomal lipid hydrolysis. J Biol Chem. 1981;256(6):2952–7.
40. Settembre C, De Cegli R, Mansueto G, et al. TFEB controls cellular lipid metabolism through a starvation-induced autoregulatory loop. Nat Cell Biol. 2013;15(6):647–58.
41. Raben N, Puertollano R, TFEB. and TFE3: Linking lysosomes to cellular adaptation to stress. Annu Rev Cell Dev Biol. 2016;32(255– 78.
42. O'Rourke EJ, Ruvkun G. MXL-3 and HLH-30 transcriptionally link lipolysis and autophagy to nutrient availability. Nat Cell Biol. 2013;15(6):668–76.
43. Hao Y, Kacal M, Ouchida AT, et al. Targetome analysis of chaperone-mediated autophagy in cancer cells. Autophagy. 2019;15(9):1558–71.

Publisher's note